Volcanic ash as an oceanic iron source and sink

Nicholas Rogan[1,2]*, Eric P. Achterberg[1], Frederic A. C. Le Moigne[1,3], Chris M. Marsay[4], Alessandro Tagliabue[2] and Richard G. Williams[2].

[1]GEOMAR Helmholtz Centre for Ocean Research Kiel, Wischhofstrasse 1-3, 24148 Kiel, Germany

[2]Department of Earth Ocean and Ecological Sciences, School of Environmental Sciences, University of Liverpool, Liverpool, L69 3GP, UK

[3]Ocean biogeochemistry and Ecosystems, European Way, National Oceanography Centre, Southampton, SO14 3ZH, UK

[4]Skidaway Institute of Oceanography, University of Georgia, 10 Ocean Science Circle, Savannah, GA 31411, USA.

*nrogan@geomar.de

Abstract

Volcanic ash deposition to the ocean forms a natural source of iron (Fe) to surface water microbial communities. Inputs of lithogenic material may also facilitate Fe removal through scavenging. Combining dissolved Fe (dFe) and thorium-234 observations alongside modelling, we investigate scavenging of Fe in the North Atlantic following the Eyjafjallajökull volcanic eruption. Under typical conditions biogenic particles dominate scavenging, whereas ash particles dominate during the eruption. The size of particles is important as smaller scavenging particles can become saturated with surface-associated ions. Model simulations indicate that ash deposition associated with Eyjafjallajökull likely led to net Fe removal. Our model suggests a three-fold greater stimulation of biological activity if ash deposition had occurred later in the growing season when the region was Fe-limited. The implications of ash particle-scavenging, eruption timing and particle saturation need to be considered when assessing the impact of ash deposition on the ocean Fe cycle and productivity.

Key points:

1. Volcanic ash deposition can lead to elevated Fe scavenging

2. Timing of an eruption determines magnitude of biological response to Fe

3. Biological control of particle scavenging breaks down during lithogenic particle deposition events

1. Introduction

The Iceland and Irminger Basins of the high latitude North Atlantic (HLNA) typically exhibit a phytoplankton growth cycle with a pronounced spring bloom commencing in April, peaking in June [*Sanders et al.,* 2005] and decaying into the autumn [*Henson et al.,* 2013]. The Iceland Basin features residual macronutrient concentrations (2-4 µM) following the spring bloom [*Sanders et al.,* 2005], which have been attributed to limitation of phytoplankton growth by iron (Fe) [*Nielsdóttir et al.,* 2009]. Accordingly, primary production and subsequent carbon export are likely to be enhanced by an increased Fe supply [*Le Moigne et al.,* 2014; *Nielsdóttir et al.,* 2009; *Ryan-Keogh et al.,* 2013].

The eruption of the Eyjafjallajökull volcano in Iceland started on April 14th 2010, and continued for five weeks, discharging ~270 ± 70 x 10^6 m^3 of ash particles into the atmosphere [*Gudmundsson et al.,* 2012]. The eruption caused a major ash deposition event in the HLNA resulting in significant biogeochemical perturbations to the Iceland Basin [*Achterberg et al.,* 2013] and sporadic ash supply to the adjacent Irminger Basin [*Stohl et al.,* 2011]. This ash deposition is thought to have stimulated phytoplankton growth and increased nutrient drawdown of the Iceland Basin to very low nitrate concentrations, < 1 µM [*Achterberg et al.,* 2013], among the lowest ever observed in the region. A study of the Irminger Basin also highlighted the role of anomalous winds, associated with an extremely negative state of the North Atlantic Oscillation in 2009-2010 in driving the anomalous phytoplankton growth [*Henson et al.,* 2013], but only for western and central parts of the basin. The fertilising effect of the ash was low compared to traditional bioassay additions of inorganic Fe (FeCl₃) [*Ryan-Keogh et al.,* 2013; *Achterberg et al.,* 2013], which produced a chlorophyll increase 10-25 times greater per unit Fe. The relatively weak response to ash suggests that additional processes restrict the efficiency of ash-derived Fe to sustain phytoplankton growth.

The removal of Fe through particle scavenging forms an important, poorly constrained, process in the oceanic Fe cycle [*Balistrieri et al.,* 1981]. Control of trace metal scavenging by sinking biogenic particles [*Siddall et al.,* 2005; *Luo & Ku,* 1999] and dust-derived lithogenic particles [*Ye et al.,* 2011] has been demonstrated, thus ash deposition may act as an Fe sink. However, quantifying the Fe removal processes is challenging due to the inherent uncertainties of the scavenging processes [*Cullen et al.,* 2006; *Wu et al.,* 2001]. The scavenging of Fe is thought to be similar to that for thorium [*Bruland & Lohan,* 2004]. Thorium-234 (^{234}Th) is often used to derive particle export in aquatic systems [*Buesseler et al.,* 1992], but can also provide information on the Fe cycle. Integrating thorium isotope observations (^{230}Th and ^{232}Th) reduces uncertainties related to steady-state assumptions and, when combined with Fe/Th ratios, permits the derivation of dFe residence times and fluxes [*Hayes et al.,* 2015]. Following Honeyman et al. (1988), we use the combination of ^{234}Th and ^{238}U data to understand the scavenging of Fe, by evaluating (1) the net adsorption rate: rate of ^{234}Th transfer from the dissolved pool to the particulate pool, and (2) the net fallout rate: the vertical removal rate of particulate scavenged ^{234}Th. In addition, the size fraction of particles in the water column is important for scavenging, since smaller particles are likely to have a larger role in the adsorption of trace metals [*Zhang et al.,* 2005].

At present, we do not clearly understand whether ash deposition acts as an Fe source or sink. Moreover, our ability to constrain how the prevailing biogeochemical conditions affect the adsorption and fallout rates of Fe is lacking. By combining observations of ^{234}Th and ^{238}U, we compare typical conditions and a volcanic ash deposition event in the HLNA to assess the relative roles of biogenic and lithogenic particles in controlling particle scavenging (Figure 1a) and the role of different particle size fractions. Using an idealised one-dimensional water

column model, we challenge the presumption that volcanic ash deposition to the surface ocean provides a net Fe supply by including the ash-derived particle scavenging and exploring the importance of eruption timing on the biogeochemical response.

2. Determining the drivers of scavenging

2.1. Data acquisition and analysis

In order to assess the relative importance of biogenic particle and atmospheric mineral aerosol control on particle scavenging and explore the importance of particle size fractionation, a range of data were required. Size-fractionated (1-53 µm and >53 µm) [234]Th, particulate organic carbon (POC), biogenic silica (BSi) and calcite ($CaCO_3$) data from depths of 50 and 150 m, were obtained using *in situ* high volume pumps (Challenger Oceanic) [*McDonnell et al.,* 2015] in spring and summer 2010 in the HLNA (RRS *Discovery* spring cruise, D350 from 26 April to 9 May, and summer cruise, D354 from 4 July to 11 August) (Figure 1b and 1c); methods described in Le Moigne et al. (2013) and Le Moigne et al. (2014). Details of sampling and analysis for dFe (< 0.2 µm), particulate Fe (pFe) species and lithogenic particles are described elsewhere [*Achterberg et al.,* 2013; *Marsay,* 2012]. The rates of adsorption (k'_f) and fallout (λ_{fal}) for [234]Th are diagnosed from the activities of dissolved and particulate [234]Th following Honeyman et al., (1988). Using the decay constant for thorium (λ_{Th}) and an assumption of chemical equilibrium we calculate rates from

$$k'_f = \frac{\lambda_{Th} A_U - \lambda_{Th} A_{Th_{diss}} + k_r A_{Th_{part}}}{A_{Th_{diss}}}, \quad (1)$$

$$\lambda_{fal} = \frac{k'_f A_{Th_{diss}} - \lambda_{Th} A_{Th_{part}} - k_r A_{Th_{part}}}{A_{Th_{part}}}. \quad (2)$$

Here k'_f is the specific adsorption rate (d^{-1}), λ_{fal} is the specific fallout rate for [234]Th (d^{-1}), $A_{Th_{diss}}$ is the activity of dissolved [234]Th, defined as the rate of change of dissolved [234]Th,

$A_{Th_{diss}} \equiv \frac{\partial[Th_{diss}]}{\partial t} \equiv \lambda_{Th}[Th_{diss}]$, $A_{Th_{part}}$ is the activity or rate of change of particle-associated [234]Th and A_U is the rate of change of [238]U; the activities are measured in decays per day per litre (dpd l[-1]). The equilibrium relationships in (1) and (2) involve a balance between supply of dissolved [234]Th from [238]U decay represented by $\lambda_{Th}A_U$, the decay of dissolved [234]Th represented by $\lambda_{Th}A_{Th_{diss}}$, the desorption of [234]Th from particles represented by $k_r A_{Th_{part}}$, the adsorption of dissolved [234]Th onto particles represented by $k'_f A_{Th_{diss}}$ and the decay of particle-associated [234]Th represented by $\lambda_{Th}A_{Th_{part}}$; all of these terms are in dpd l[-1] d^{-1}. The diagnostics of k'_f and λ_{fal} for [234]Th are then taken to be appropriate for Fe, due to their similar behaviour in the surface ocean [*Hayes et al.,* 2015]. The pFe samples were collected concurrently with particulate [234]Th using the *in situ* high volume pumps (Challenger Oceanic) and ash deposition fields were diagnosed from the characteristics of the source material together with an atmospheric Lagrangian dispersion model and satellite data [*Stohl et al.,* 2011]. To take into account the timescale of particle sinking we use a lag in the ash deposition fields in order to compare scavenging rates with an appropriate ash supply. The relative importance of each size class is calculated by substituting activities for each particular size class into (1) and (2). Statistical analysis is carried out using non-parametric methods; the Wilcoxon Rank Sum test is used to determine whether datasets are significantly different, giving W, and Spearman's Rank Correlation coefficient is used to measure correlation, denoted by ρ.

2.2. How does volcanic ash affect fallout rates?

The prevailing view is that removal of trace elements by scavenging is driven by biogenic particle production and leads to a particle fallout flux from the upper water column, at a specific fallout rate (λ_{fal}) [*Siddall et al.,* 2005; *Luo & Ku,* 1999]. This viewpoint is tested by

comparing data collected during summer 2010 (Figure 1b) with the Eyjafjallajökull volcanic eruption during spring 2010 (Figure 1c|). The mean fallout rates of [234]Th during the volcanic eruption in spring are double those seen for the summer, 0.25 ± 0.13 compared to 0.13 ± 0.07 d^{-1} respectively (W = 289, p < 0.02), indicating a faster removal of [234]Th coinciding with the ash deposition. During the ash deposition the fallout rates are not correlated with calcite concentrations, an indication of biogenic particle abundance, but the rates are positively correlated with calcite under "typical " conditions during the summer ($\rho = 0.58$, p < 0.01, Figure 2a). The observed fallout rates at 150 m (Figure 2b) in spring 2010 are related to ash deposition to the surface ocean ($\rho = 0.89$ p < 0.01). The fallout rates of small (1-53 µm, $\rho = 0.86$, p < 0.03) and large (>53 µm, $\rho = 0.86$, p < 0.03) particles are correlated with ash deposition (Figure 2c) on sinking timescales of 9 and 3 days respectively. The observations of fallout rates, the traditional measure of particle removal, thus support the hypothesis that biogenic particles are important for setting removal rates under typical conditions, but ash particle supply determines the removal rates during a volcanic eruption.

2.3. How does volcanic ash affect adsorption rates?

A key loss process for the dissolved trace metals in the water column is specific net adsorption rate (k'_f); the rate at which dissolved elements become associated with particulate material prior to vertical fallout. The specific net adsorption rates increased four fold from 0.0052 ± 0.0026 d^{-1} during the period of ash deposition in spring to 0.019 ± 0.017 d^{-1} in the summer after the eruption (W = 190, p < 0.03). There is a strong positive correlation between calcite concentration and specific net adsorption rate ($\rho = 0.80$, p <<0.01) under typical conditions (Figure 3a), but this relationship breaks down during the ash deposition. There is a moderate correlation between specific net adsorption rate and ash deposition ($\rho = 0.43$, p < 0.09) (Figure 3b). However, if lithogenic particle concentrations are used to normalise

specific net adsorption rate, a stronger correlation emerges between the normalised adsorption rates $((\mu g\ L^{-1})^{-1}\ d^{-1})$ and ash deposition ($\rho = 1$, $p < 0.02$) (Figure 3c). This latter correlation suggests that ash particles control water column adsorption rates during periods of ash deposition. At 150m this relationship is observed for large particle normalised adsorption rates ($\rho = 1$, $p < 0.02$) (Figure 3d), but is not significant for small particle adsorption rates ($\rho = 0.9$, $p < 0.09$). The specific net adsorption rates resulting from biogenic particles are higher than those for ash particles, and how this links to absolute scavenging removal fluxes is discussed in Section 2.5.

2.4. How does the scavenging response differ for small versus large particles?

Our analyses find both small and large particles are effective in enhancing fallout, but only large particles are effective in adsorbing ^{234}Th at a depth of 150m. This challenges the expectation that smaller particles, with larger ratios of surface area to volume, should have a higher adsorption affinity for dissolved ions. These views can be reconciled if the slower sinking rates of small particles versus faster sinking rates of large particles are taken into account. Small particles can initially act as the strongest scavengers, but the surface sites of the small particles may become saturated with metals during their relatively slow descent to 150 m in our study system. Support for this view is derived from the strong decline in lithogenic particle normalised adsorption rates between 50m and 150m for the small particles (42 to 12 $(g\ m^{-3})^{-1}\ d^{-1}$); the decline is smaller for large particles (17 to 10 $(g\ m^{-3})^{-1}\ d^{-1}$).

2.5. Derived Fe removal rates and fluxes

As Fe and Th are both scavenged elements [*Hayes et al.,* 2015; *Whitfield & Turner,* 1987; *Clegg & Sarmiento,* 1989; *Anderson,* 2014], we can use our results from ^{234}Th to make an appraisal of the likely changes in Fe adsorption and fallout between periods with and without

ash deposition. We assume adsorption rates of Fe can be quantified via the dFe pool, which actively associates with particles (>1 μm) through processes such as colloidal aggregation and surface association [*Honeyman & Santschi,* 1989]. The fallout rates of Fe are assessed using the leachable pFe (determined using an acetic acid-hydroxylamine leach on the particles collected from the high volume pumps), which may underestimate the total adsorbed metal [*Rauschenberg & Twining,* 2015]).

Adsorption rates of Fe onto particles during the spring volcanic eruption and subsequent summer are 1.03 $\pm$ 0.89 and 7.14 $\pm$ 5.9 pM Fe d^{-1}, respectively (W = 52, p < 0.005). The difference between specific net adsorption rates of ash particles and biogenic particles (Section 2.3) is further increased by higher observed dFe concentrations in summer. However, higher concentrations of particles and pFe in spring resulted in greater overall Fe fallout rates during the ash deposition period (26.9 $\pm$ 63 pM Fe d^{-1}, compared to 1.3 $\pm$ 1.7 pM Fe d^{-1} during summer without ash deposition (W = 161, p < 0.001). Vertical integration between depths of 50m and 150m yields a pFe flux out of the upper 150 m of 2.69 $\pm$ 6.3 μmol Fe m^{-2} d^{-1} in spring (during the eruption), which is much greater than the summer flux of 0.13 $\pm$ 0.17 μmol Fe m^{-2} d^{-1}. Our summer estimates for typical conditions compare reasonably well to independent estimates of Fe removal, thereby providing confidence in our estimates. For example, in the study region, fluxes of total pFe in summer were 0.56 $\pm$ 0.16 μmol Fe m^{-2} d^{-1}, as measured by a neutrally buoyant sediment trap at 150 m [*Marsay,* 2012]. Additionally, in a different dynamical regime, dFe from dust fluxes at 150 m from the Hawaii Ocean Time-series station ALOHA ranged from 0.06 to 0.22 μmol Fe m^{-2} d^{-1} derived from integrated [230]Th residence times, [*Hayes et al.,* 2015] .

Assuming the spring fallout rates are valid for the duration of ash deposition, integrating over

the surface area of the Iceland Basin (~5 x 10^5 km^2) and the period of significant volcanic activity (~21 days [*Stohl et al.,* 2011]), yields a total removal of 28 ± 66 Mmol of Fe compared to a removal of 1.4 ± 1.8 Mmol Fe over the summer. Our estimate for the spring removal compares well with the total Fe supply by volcanic ash of 1.43 to 31.4 Mmol Fe [*Achterberg et al.,* 2013] that is derived from Fe dissolution related to ash salt-layer thickness calculations. Our spring removal estimate is greater than the estimated bioavailable dFe supply, 0.55 to 1.80 Mmol Fe [*Achterberg et al.,* 2013], that is derived from experimentally determined Fe solubility measurements. The instantaneous solubility of Fe is a parameter that takes into account any Fe that precipitates out of solution due to the Fe concentrations exceeding Fe solubility, as modified by organic Fe binding ligands, in seawater [*Gledhill & Buck,* 2012]. This precipitate is included in our pFe data, thus our net scavenging removal fluxes include the losses of insoluble ash Fe. The Fe losses are up to two orders of magnitude larger than the bioavailable Fe supply. Hence, our results suggest that the observed biological response to the Eyjafjallajökull eruption [*Achterberg et al.,* 2013] was lower than might have been anticipated due to scavenging of Fe by ash particles. Therefore, an overall Fe fertilisation from an ash deposition event requires the Fe supply to be larger than its loss of Fe arising from the enhancement of particle scavenging.

3. Modelling sensitivity of biological production to ash deposition

 In order to test our hypothesis that ash particle scavenging forms an important process in determining oceanic biogeochemical responses to volcanic eruptions, a one-dimensional biogeochemical formulation of the Massachusetts Institute of Technology General Circulation Model [*Dutkiewicz et al.,* 2005] is employed. A 1D version of the model is used as ash particle addition and residence time in the upper water column is on the timescale of a few days, thereby making horizontal processes relatively unimportant to our experiments.

The model has periodic boundaries and maintains a seasonally-repeating cycle of mixing, nutrient consumption and remineralisation by inclusion of advective supplies of heat, salt and nutrients [*Williams,* 1988].

An Eyjafjallajökull-analogue eruption was simulated using ash deposition fields [*Stohl et al.,* 2011]. The ash deposition was implemented as a single supply of ash particles to the surface ocean with an instantaneous Fe solubility of 0.1% as determined by a rapid leach experiment on the ash [*Achterberg et al.,* 2013]. In addition to Fe supply, the ash particles were explicitly represented using small (1-53 μm) and large (>53 μm) ash-particle size classes with specific particle concentration dependent scavenging rates, which were constrained by the observational data (supplementary information). Ash particle scavenging was added to the traditional scavenging closure, accounting for the role of biogenic particles, climatological lithogenic dust supply and colloidal aggregation in removing Fe from the dissolved pool. A control model run (without additional Fe supply or ash-derived processes) was compared to two model closures that resolved the volcanic ash deposition event: one including additional ash-derived scavenging (SCAV) and another without additional ash-derived scavenging (NO-SCAV). Further information on model formulation and diagnostics is included in the supplementary information.

In our model, additional ash-derived scavenging is required in order to reproduce observed surface dFe concentrations (Figure 4a). Notably, removing ash scavenging yields dFe concentrations that are too high and persist for too long (Figures 4a and S2c). The ash scavenging simulation reveals that there is a strong increase in biological Fe uptake, although the ash scavenging removal of Fe is intermittently a more dominant process (Figure 4b). For the duration of the eruption the ash scavenging is responsible for 50% of the total Fe removed

from the surface Fe pool (the sum of net ash scavenging, net biological uptake and net traditional scavenging, Figure 4c) and peaks at almost 100% when deposition rates are high. For most of the eruption, Fe inputs (summed from dust deposition, ash deposition, advective supplies and ash particle desorption) were greater than Fe removal (Figure 4d), but when ash deposition was low the removal of Fe was greater than the supply. During this period of low ash deposition, the ash scavenging was as important for the removal of Fe from the surface water as biological uptake (Figure 4c).

The Eyjafjallajökull eruption took place at the onset of the 2010 spring bloom, when macronutrients and dFe were replete. Our model suggests that the largest biological response to ash deposition would be observed when ash deposition occurs later in the season, coincident with seasonal Fe limitation and when there are residual macronutrients in the surface waters (Figure S3a and S3b). For example, the change in dFe concentration is much greater if an eruption is simulated in September (Figure 4a). A September ash deposition event leads to a greater increase in biological Fe uptake (Figure 4b), but a much lower level of ash scavenging, both in absolute and proportional terms (Figures 4b and S3c). Later in the season the ash deposition also sustains a higher proportion of Fe supply for a longer period (Figure S3d). The relative importance of the scavenging by ash particles is dependent on the timing of the ash deposition relative to the biogeochemical environment. For the September simulation, biological Fe uptake forms a larger sink for dFe as Fe stimulates biological activity during this period. Consequently, the amount of Fe that is removed by ash scavenging is reduced due to the increase in biological Fe uptake.

4. Conclusions

Volcanic ash deposition provides both a source and a sink of Fe in the surface ocean. The prevailing biogeochemical conditions of the receiving waters determine the biological response to ash supply. Our approach of using ^{234}Th radioisotopes to quantify particle scavenging rates confirms that biogenic particles are important for Fe removal during typical conditions and that the specific net adsorption rates are stronger for biogenic particles relative to ash particles. However, removal fluxes of Fe out of the upper 150m during the volcanic eruption were twenty times higher than under typical conditions. The size of particles is important as smaller scavenging particles can become saturated with surface-associated ions in highly loaded systems. This analysis, supported by an idealised modelling study, suggests that the overall impact of a volcanic ash deposition event cannot be measured solely by the net supply of bioavailable Fe, instead the timing of the event relative to the biogeochemical environment is crucial. The biogeochemical response in the HLNA to ash deposition is likely to vary from being almost negligible during winter to a high sensitivity towards the end of the growing season when macronutrients are replete and the system is Fe-limited. This analysis implies that the observed biological response to the Eyjafjallajökull volcanic eruption was tempered by ash scavenging of Fe. Therefore, an ash deposition event need not automatically lead to a net increase in biological activity.

5. Acknowledgments

assistance. We are also grateful for constructive comments from two anonymous reviewers.

6. References

Achterberg, E.P. et al., 2013. Natural iron fertilization by the Eyjafjallaj{ö}kull volcanic eruption. *Geophys. Res. Lett.*, 40(5), pp.921–926.

Anderson, R.F., 2014. Chemical tracers of particle transport. In *Treatise on Geochemistry (Second Edition)*. pp. 259–280.

Balistrieri, L., Brewer, P. & Murray, J., 1981. Scavenging residence times of trace metals and surface chemistry of sinking particles in the deep ocean. *Deep Sea Research Part A.*, 28, pp.101–121.

Bruland, K.W. & Lohan, M.C., 2004. Controls of Trace Metals in Seawater. *Treatise Geochemistry*, 6, pp.23–47.

Buesseler, K.O. et al., 1992. Carbon and Nitrogen Export during the Jgofs North-Atlantic Bloom Experiment Estimated from Th-234u-238 Disequilibria. *Deep Sea Research Part A. Oceanographic Research Papers*, 39(7-8), pp.1115–1137.

Clegg, S.L. & Sarmiento, J.L., 1989. The hydrolytic scavenging of metal ions by marine particulate matter. *Progress in Oceanography*, 23, pp.1–21.

Cullen, J.T., Bergquist, B.A. & Moffett, J.W., 2006. An assessment of particulate organic carbon to thorium-234 ratios in the ocean and their impact on the application of Th-234 as a POC flux proxy. *Marine Chemistry*, 98, pp.203–295.

Dutkiewicz, S. et al., 2005. *A three-dimensional ocean-seaice-carbon cycle model and its coupling to a two-dimensional atmospheric model: uses in climate change studies*,

Gledhill, M. & Buck, K.N., 2012. The Organic Complexation of Iron in the Marine Environment: A Review. *Front. Microbio.*, 3(69).

Gudmundsson, M.T. et al., 2012. Ash generation and distribution from the April-May 2010 eruption of Eyjafjallajökull, Iceland. *Scientific Reports*, 2(572).

Hayes, C.T. et al., 2015. Thorium isotopes tracing the iron cycle at the Hawaii Ocean Time-series station ALOHA. *Geochimica et Cosmochimica Acta*, 169, pp.1–16.

Henson, S.A. et al., 2013. Unusual subpolar north Atlantic phytoplantkon bloom in 2010: Volcanic fertilization or North Atlantic Oscillation? *Journal of Geophysical Research: Oceans*, 118, pp.4771–4780.

Honeyman, B., Balistrieri, L. & Murray, J., 1988. Oceanic trace metal scavenging: the importance of particle concentration. *Deep Sea Research Part A.*, 35(2), pp.227–246.

Honeyman, B. & Santschi, P., 1989. A Brownian-pumping model for oceanic trace metal scavenging: Evidence from Th isotopes. *Journal of marine research*, 47(42), pp.951–

992.

Luo, S. & Ku, T.-L., 1999. Oceanic 231Pa=230Th ratio influenced by particle composition and remineralization. *Earth and Planetary Science Letters*, 167, pp.183–195.

Marsay, C.M., 2012. *Particulate trace metals, Carbon and Nitrogen in the mesopelagic*. School of Ocean and Earth Science, University of Southampton, UK.

McDonnell, A.M.P. et al., 2015. The oceanographic toolbox for the collection of sinking and suspended marine particles. *Progress in Oceanography*, 133, pp.17–31.

Le Moigne, F. a C. et al., 2013. Export of organic carbon and biominerals derived from 234Th and 210Po at the Porcupine Abyssal Plain. *Deep-Sea Research Part I*, 72, pp.88–101.

Le Moigne, F. a C. et al., 2014. Sequestration efficiency in the iron-limited North Atlantic: Implications for iron supply mode to fertilized blooms. *Geophysical Research Letters*, 41(13), pp.4619–4627.

Nielsdóttir, M.C. et al., 2009. Iron limitation of the postbloom phytoplankton communities in the Iceland Basin. *Global Biogeochem. Cycles*, 23(3), p.GB3001.

Rauschenberg, S. & Twining, B.S., 2015. Evaluation of approaches to estimate biogenic particulate trace metals in the ocean. *Marine Chemistry*, 171, pp.67–77.

Ryan-Keogh, T.J. et al., 2013. Spatial and temporal development of phytoplankton iron stress in relation to bloom dynamics in the high-latitude North Atlantic Ocean. *Limnology and Oceanography*, 58(2), pp.533–545.

Sanders, R. et al., 2005. New production in the Irminger Basin during 2002. *Journal of Marine Systems*, 55(3-4), pp.291–310.

Siddall, M. et al., 2005. 231Pa/230Th fractionation by ocean transport, biogenic particle flux and particle type. *Earth and Planetary Science Letters*, 237, pp.135–155.

Stohl, A. et al., 2011. Determination of time-and height-resolved volcanic ash emissions and their use for quantitative ash dispersion modeling: the 2010 Eyjafjallajökull eruption. *Atmospheric Chemistry and Physics*, 11, pp.4333–4351.

Whitfield, M. & Turner, D.R., 1987. The role of particles in regulating the composition of seawater. In W. Stumm, ed. *Aquatic Surface Chemistry*. New York: Wiley, pp. 457–493.

Williams, R.G., 1988. Modification of ocean eddies by air-sea interaction. *Journal of Geophysical Research*, 93(C12), pp.15523–15533.

Wu, J. et al., 2001. Soluble and Colloidal Iron in the Oligotrophic North Atlantic and North Pacific. *Science*, 293, pp.847–849.

Ye, Y. et al., 2011. Dust deposition: Iron source or sink? A case study. *Biogeosciences*, 8(8), pp.2107–2124.

Zhang, L. et al., 2005. Size-fractionated thorium isotopes (228Th, 230Th, 232Th) in surface waters in the Jiulong River estuary, China. *Journal of Environmental Radioactivity*, 78, pp.199–216.
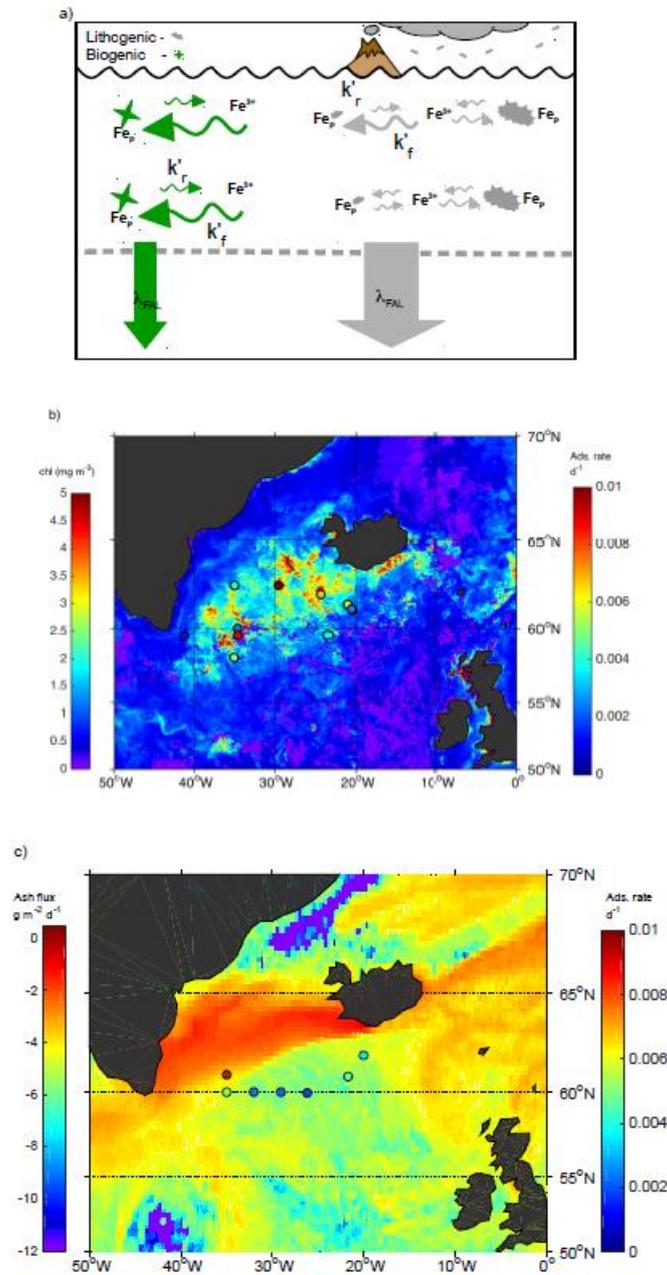
Figure 1. a) Schematic illustrating how scavenging operates under 'typical' circumstances (green arrows) and during an eruption (grey arrows), b) Contour plot of MODIS/AQUA 4km monthly mean satellite chlorophyll-*a* concentration (mg m^{-3}) for July 2010 overlaid with calculated adsorption rates (d^{-1}) for the same period, c) contour plot of ash deposition (log g m^{-2} d^{-1}) on 25th April 2010 overlaid with calculated adsorption rates (d^{-1}) between 1st and 7th May 2010.
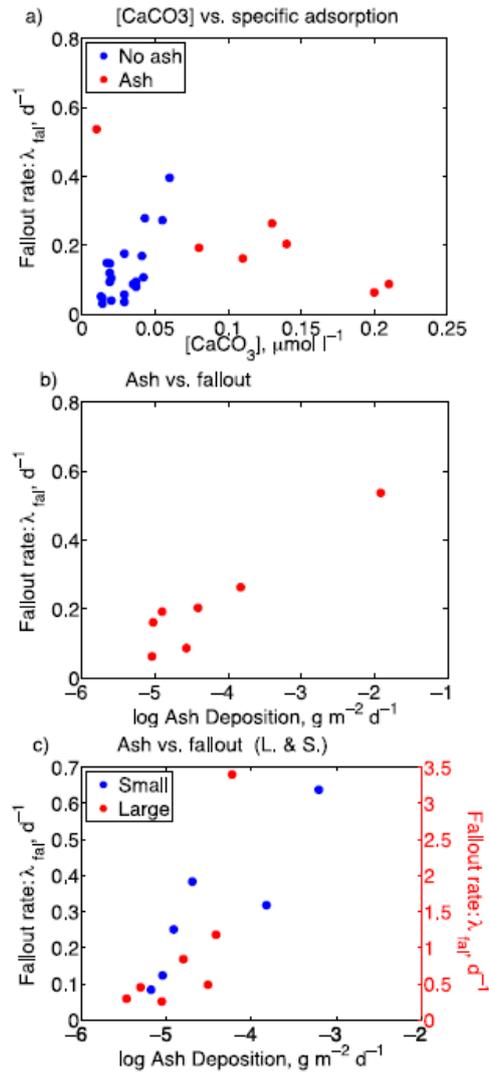
Figure 2 a) Relationship between calcite concentration ($CaCO_3$ in μmol L^{-1}) and fallout rates (d^{-1}) in periods with and without ash deposition ($\rho = 0.58$, $p < 0.01$), b), relationship between log ash deposition (g m^{-2} d^{-1}) and fallout rates (d^{-1}) during the volcanic eruption ($\rho = 0.89$, $p < 0.01$), c) relationship between fallout rates (d^{-1}) of small (1-53 μm) and large (>53 μm) particles and ash deposition rate (g m^{-2} d^{-1}) (both, $\rho = 0.86$, $p < 0.03$) with lags of 9 and 3 days respectively, note the second y-axis (For clarity we do not plot the full range on panel c); for full figure see Figure S1b).
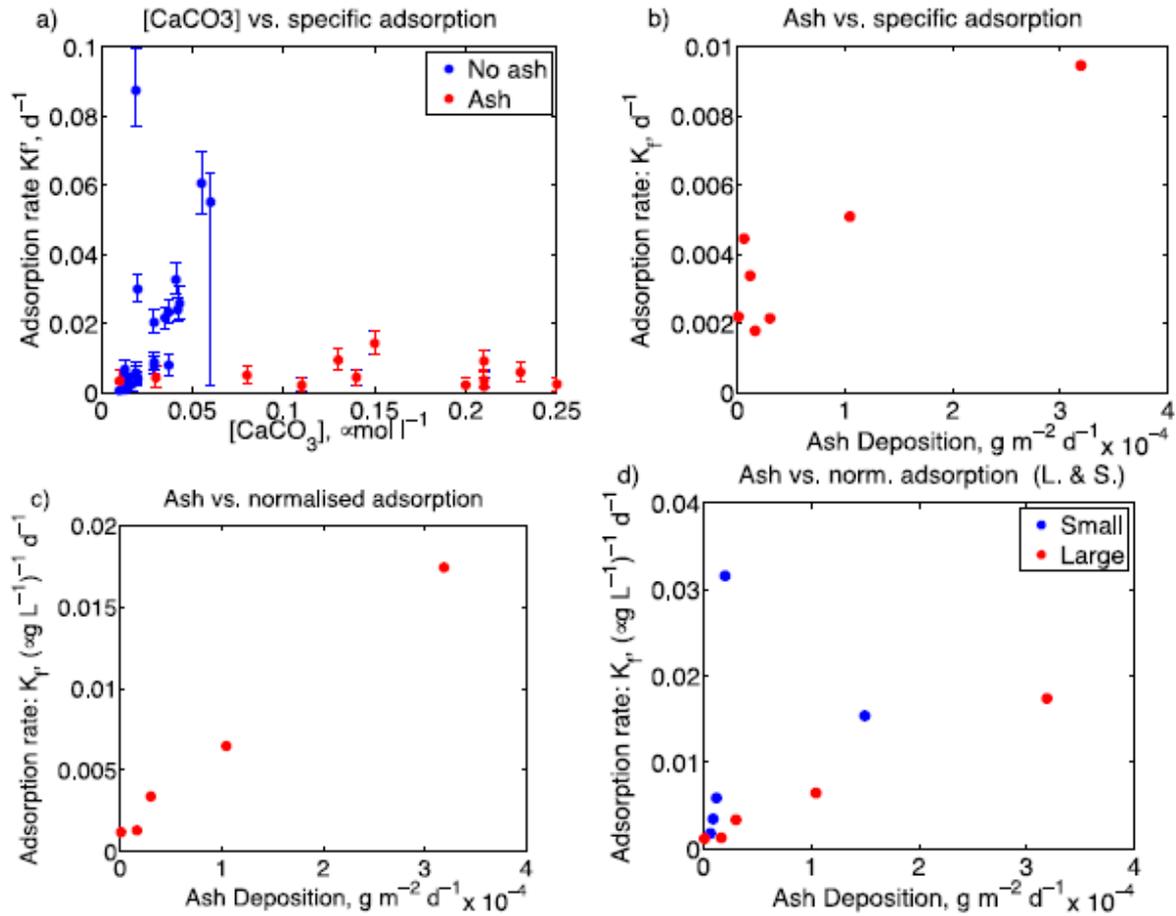
Figure 3 a) Relationship between calcite concentration ($CaCO_3$ in μmol L^{-1}) and adsorption rates (d^{-1}) in periods with and without ash deposition ($\rho = 0.80$, $p < <0.01$), b) relationship between adsorption rate (d^{-1}) and ash deposition rate (g m^{-2} d^{-1}) ($\rho = 0.43$, not significant), c) relationship between lithogenic particle normalised adsorption rate ((μg L^{-1})$^{-1}$ d^{-1}) and ash deposition rate (g m^{-2} d^{-1}) ($\rho = 1$, $p < 0.02$), d) relationship between lithogenic particle normalised adsorption rate ((μg L^{-1})$^{-1}$ d^{-1}) of small (1-53 μm) ($\rho = 0.9$, not significant $p < 0.09$) and large (>53 μm) ($\rho = 1$, $p < 0.02$) particles and ash deposition rate (g m^{-2} d^{-1}) with lags of 9 and 3 days respectively.
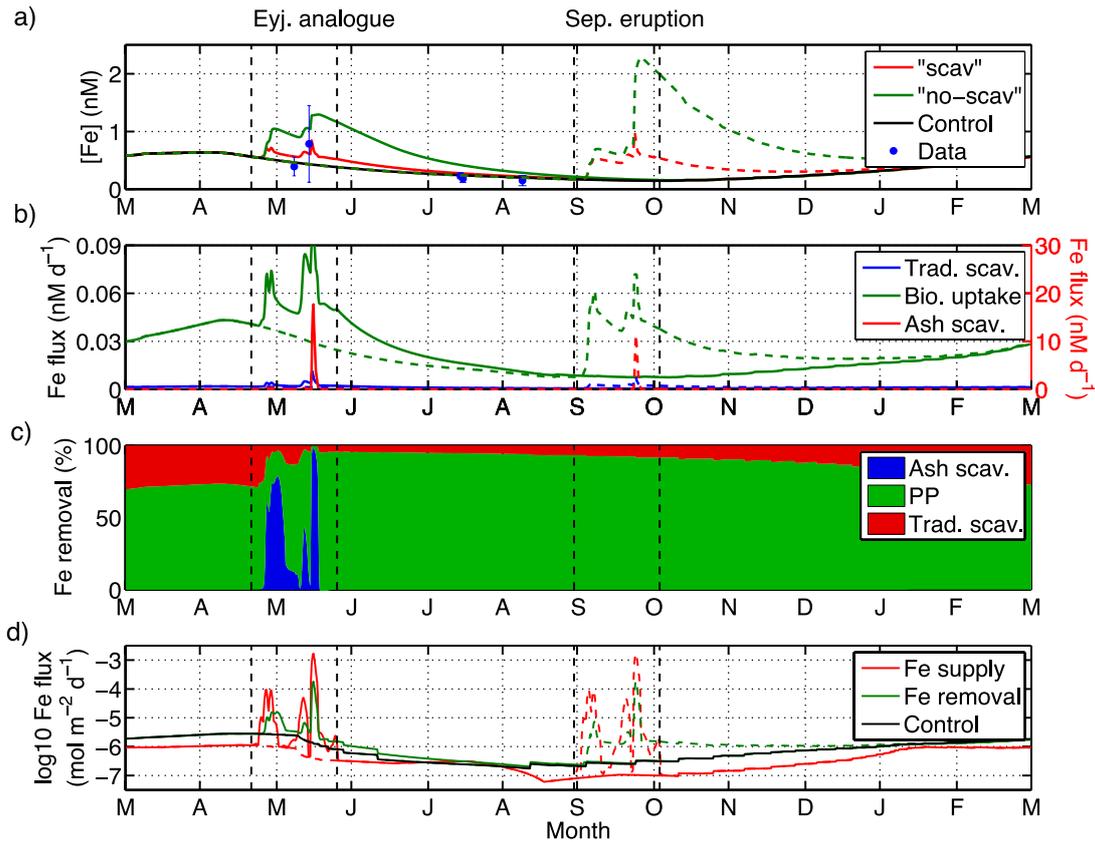
Figure 4. a) Modelled surface dFe concentrations, from simulations with (SCAV, red lines) and without (NO-SCAV, green lines) ash-derived scavenging and from the Eyjafjallajökull-analogue (solid line) and September eruption (dashed line) simulations, with dFe data (both integrated down to 50 m) over one year, b) surface mixed-layer Fe removal fluxes (note ash scavenging on second y-axis) over one year for the Eyjafjallajökull-analogue (solid line) and September-eruption (dashed line) simulations (both using the SCAV closure), c) area plot showing relative contributions to dFe removal processes in the surface mixed-layer over a year for the Eyjafjallajökull-analogue, d) gross Fe supply and Fe removal terms in the surface mixed-layer for the Eyjafjallajökull-analogue (solid line) and September eruption (dashed line) simulations (both using SCAV closure). The timing of the two simulations examined are indicated with dashed lines and labelled in the top panel.